

## Supporting Information for

# Effect of secondary substituent on the physical properties, crystal structures, and nanoparticle morphologies of (porphyrin)Sn(OH)2: diversity enabled via synthetic manipulations

Suk Joong Lee, Rebecca A. Jensen, Christos D. Malliakas, Mercouri G. Kanatzidis, Joseph T. Hupp,\* and SonBinh T. Nguyen

*Department of Chemistry,  
Northwestern University, 2145 Sheridan Road, Evanston, Illinois 60208-3111, USA*

## I. Materials

All other chemicals were obtained from commercial sources and used without further purification. All of the reactions and manipulations of the porphyrin building blocks were carried out under N<sub>2</sub> with the use of standard inert-atmosphere and Schlenk techniques unless otherwise noted. Microwave reactions were carried out using an Initiator Microwave Synthesizer from Biotage. Solvents used in inert-atmosphere reactions were dried and degassed using standard procedures. Flash column chromatography was carried out with 230-400 mesh silica gel from Aldrich using the wet-packing method. All deuterated solvents were purchased and used as received from Cambridge Isotopes Laboratories.

## II. Instrumentations

NMR spectra were recorded on a Varian Inova 500 (499.773 MHz for <sup>1</sup>H and 125.669 MHz for <sup>13</sup>C) spectrometer. <sup>1</sup>H chemical shifts are referenced to the proton resonance resulting from protic residue in deuterated solvent and <sup>13</sup>C chemical shifts recorded downfield in ppm relative to the carbon resonance of the deuterated solvents. Absorbance and emission spectra were obtained using a Varian Cary 5000 UV-Vis-NIR spectrophotometer and a Jobin Yvon SPEX Fluorolog fluorometer using quartz cells. Matrix-Assisted Laser-Desorption-Ionization Time-of-flight Mass Spectra (MALDI-TOF) were obtained on a PE Voyager DE-Pro MALDI-TOF Mass Spectrometer in the Analytical Services Laboratory at Northwestern University.

All scanning electron microscopy (SEM) images were obtained using a LEO Gemini 1525 SEM (Electron Probe Instruments Center (EPIC), NUANCE, Northwestern University). All fluorescence microscopy images were obtained using a Zeiss AxioPhot epifluorescence microscope (Carl Zeiss, GmbH, Jena, Germany) equipped with fluorescein isothiocyanate (FITC) and tetramethyl rhodamine isocyanate filter sets and a Zeiss AxioCam camera for image acquisition.

Powder X-ray diffraction measurements were recorded with a Rigaku XDS 2000 diffractometer using nickel-filtered Cu K $\alpha$  radiation ( $\lambda = 1.5418 \text{ \AA}$ ) over a range of  $5^\circ < 2\theta < 65^\circ$  and an X'Celerator detector operating at 45 kV and 40 mA. Particle size and size distribution in solution were performed with a BI-200SM Goniometer with BI-9000 AT Digital Correlator from Brookhaven Instrument.

## III. Synthesis

**General procedure for the synthesis of dipyrromethanes.** The dipyrromethanes were synthesized according to modified literature procedures.<sup>1</sup> In a typical reaction, 2,6-dialkoxybezaldehyde (10 mmol) was dissolved in freshly distilled pyrrole (250 mmol, 25 equiv) in a 100-mL round-bottom flask equipped with a magnetic stirbar. The mixture was degassed for 10 min and trifluoroacetic acid (TFA, 1 mmol, 0.1 equiv) was injected into the reaction via syringe. The resulting mixture was stirred for 10 min under N<sub>2</sub>. After quenching the reaction with aqueous sat. NaOH solution (5 mL), ethylacetate (15 mL) was added.

The mixture was washed with water (2 x 50 mL), dried over anhydrous magnesium sulfate, and concentrated to dryness using a rotary evaporator. The resulting oily residue was purified by silica-gel column chromatography (hexanes/ethylacetate 8.5:1.5 v/v) to afford colorless oil.

**Meso-(2,6-bis(methoxy)phenyl)dipyrromethane.** A colorless oil (1.75 g, 62% yield).  $^1\text{H}$  NMR ( $\text{CDCl}_3$ ):  $\delta$  8.53 (s, 1H), 7.19 (t,  $^3J_{\text{H-H}} = 8.6$  Hz, 1H), 6.64 (s, 2H), 6.62 (d,  $^3J_{\text{H-H}} = 8.6$  Hz, 2H), 6.18 (s, 2H), 6.13 (m, 2H), 5.92 (s, 2H), 3.74 (s, 6H).

**Meso-(2,6-bis(*n*-butoxy)phenyl)dipyrromethane.** A colorless oil (2.91 g, 81% yield).  $^1\text{H}$  NMR ( $\text{CDCl}_3$ ):  $\delta$  8.57 (s, 1H), 7.13 (t,  $^3J_{\text{H-H}} = 8.4$  Hz, 1H), 6.62 (s, 2H), 6.57 (d,  $^3J_{\text{H-H}} = 8.4$  Hz, 2H), 6.21 (s, 2H), 6.09 (m, 2H), 5.88 (s, 2H), 3.88 (m, 4H), 1.60 (m, 4H), 1.37 (m, 4H), 0.92 (t,  $^3J_{\text{H-H}} = 6.8$  Hz, 6H).

**Meso-(2,6-bis(*n*-octoxy)phenyl)dipyrromethane.** A colorless oil (3.7 g, 78% yield).  $^1\text{H}$  NMR ( $\text{CDCl}_3$ ):  $\delta$  8.57 (s, 1H), 7.12 (t,  $^3J_{\text{H-H}} = 8.4$  Hz, 1H), 6.61 (s, 2H), 6.56 (d,  $^3J_{\text{H-H}} = 8.2$  Hz, 2H), 6.20 (s, 2H), 6.08 (m, 2H), 5.88 (s, 2H), 3.87 (m, 4H), 1.54 (m, 4H), 1.28 (m, 24H), 0.89 (t,  $^3J_{\text{H-H}} = 6.3$  Hz, 6H).

**General procedure for the synthesis of porphyrins.** Freshly distilled 4-pyridine carboxaldehyde (2.35 mmol) and *meso*-substituted dipyrromethane (2.35 mmol) were dissolved in propionic acid (25 mL) in a 100-mL round-bottom flask equipped with a magnetic stirbar and a water-cooled reflux condenser. The mixture was then allowed to reflux for 2.5 h under air. After cooling, the reaction mixture was evaporated to dryness using a rotary evaporator to yield a dark residue, which was dissolved in dichloromethane (~10 mL). This solution was washed with saturated aqueous potassium carbonate (2 x 10 mL) and water (2 x 200 mL), dried over anhydrous magnesium sulfate, and concentrated to dryness using a rotary evaporator. The resulting residue was purified by silica-gel column chromatography (methanol/dichloromethane 5:95 v/v).

**5,15-Bis(4-pyridyl)-10,20-bis[2,6-bis(methoxy)phenyl]porphyrin (L1).** A dark red-purple solid (291 mg, 28.6% yield).  $^1\text{H}$  NMR ( $\text{CDCl}_3$ ):  $\delta$  9.01 (d,  $^3J_{\text{H-H}} = 4.9$  Hz, 4H), 8.84 (d,  $^3J_{\text{H-H}} = 4.8$  Hz, 4H), 8.75 (d,  $^3J_{\text{H-H}} = 4.9$  Hz, 4H), 8.18 (d,  $^3J_{\text{H-H}} = 5.5$  Hz, 4H), 7.74 (t,  $^3J_{\text{H-H}} = 8.6$  Hz, 2H), 7.02 (d,  $^3J_{\text{H-H}} = 8.6$  Hz, 4H), 3.52 (s, 12H), -2.68 (s, 2H).  $^{13}\text{C}\{\text{H}\}$  NMR ( $\text{CDCl}_3$ ):  $\delta$  160.65, 150.84, 148.31, 130.63, 129.65, 119.62, 115.99, 113.23, 104.41, 56.21. MS (MALDI-TOF):  $m/z = 738.2$  for  $\text{M}^+$ ; Calcd 736.8.

**5,15-Bis(4-pyridyl)-10,20-bis[2,6-bis(*n*-butoxy)phenyl]porphyrin (L2).** A dark red-purple solid (690 mg, 35% yield).  $^1\text{H}$  NMR ( $\text{CDCl}_3$ ):  $\delta$  9.01 (d,  $^3J_{\text{H-H}} = 6.2$  Hz, 4H), 8.85 (d,  $^3J_{\text{H-H}} = 4.6$  Hz, 4H), 8.71 (d,  $^3J_{\text{H-H}} = 4.6$  Hz, 4H), 8.15 (d,  $^3J_{\text{H-H}} = 6.2$  Hz, 4H), 7.69 (t,  $^3J_{\text{H-H}} = 8.4$  Hz, 2H), 6.99 (d,  $^3J_{\text{H-H}} = 8.44$  Hz, 4H), 3.84 (t,  $^3J_{\text{H-H}} = 7.1$  Hz, 8H), 0.95 (m, 8H), 0.49 (m, 8H), 0.27 (t,  $^3J_{\text{H-H}} = 7.3$  Hz, 12H), -1.94 (s, 2H).  $^{13}\text{C}\{\text{H}\}$  NMR ( $\text{CDCl}_3$ ):  $\delta$  160.16, 151.05, 148.34, 130.42, 129.74, 120.25, 115.72, 113.78, 105.20, 68.40, 30.74, 18.56, 13.42. MS (MALDI-TOF):  $m/z = 906.8$  for  $\text{M}^+$ ; Calcd 905.1.

**5,15-Bis(4-pyridyl)-10,20-bis[2,6-bis(*n*-octoxy)phenyl]porphyrin (L3).** A dark red-purple solid (354 mg, 26% yield).  $^1\text{H}$  NMR ( $\text{CDCl}_3$ ):  $\delta$  9.02 (d,  $^3J_{\text{H-H}} = 4.2$  Hz, 4H), 8.88 (d,  $^3J_{\text{H-H}} = 4.3$  Hz, 4H), 8.74 (d,  $^3J_{\text{H-H}} = 3.7$  Hz, 4H), 8.18 (d,  $^3J_{\text{H-H}} = 4.9$  Hz, 4H), 7.71 (t,  $^3J_{\text{H-H}} = 8.3$  Hz, 2H), 7.01 (d,  $^3J_{\text{H-H}} = 8.5$  Hz, 4H), 3.85 (t,  $^3J_{\text{H-H}} = 6.1$  Hz, 8H), 0.97 (m, 8H), 0.83 (m, 8H), 0.68 (m, 8H), 0.59 (m, 16H), 0.53 (t,  $^3J_{\text{H-H}} = 7.3$  Hz, 12H), 0.48 (m, 8H), -2.68 (s, 2H).  $^{13}\text{C}\{\text{H}\}$  NMR ( $\text{CDCl}_3$ ):  $\delta$  155.16, 146.09, 143.23, 125.35, 124.74, 115.30, 110.65, 108.79, 100.19, 63.70, 26.48, 23.84, 23.78, 20.43, 17.40, 8.95. MS (MALDI-TOF):  $m/z = 1130.6$  for  $\text{M}^+$ ; Calcd 1129.6.

**General procedure for the synthesis of (porphyrin)Sn(OH)<sub>2</sub>.** A solution of the free-base porphyrin (0.17 mmol) and SnCl<sub>2</sub>·2H<sub>2</sub>O (340 mg, 1.7 mmol) were refluxed in pyridine (15 mL) under air with exclusion of light for 4 h and allowed to cool to room temperature. Water (60 mL) was added, and the dark red precipitate was collected by filtration to afford Sn<sup>IV</sup> porphyrin intermediate.

Next, to a mixture of K<sub>2</sub>CO<sub>3</sub> (375 mg, 2.7 mmol) in THF (110 mL) and H<sub>2</sub>O (30 mL) was added to the aforementioned Sn<sup>IV</sup> porphyrin intermediate under air. The resulting mixture was refluxed for 4 h with exclusion of light. After evaporating the THF, the product was extracted with CHCl<sub>3</sub> (3 x 10 mL). The combined organics were washed with H<sub>2</sub>O (30 mL), dried over MgSO<sub>4</sub> and evaporated to afford a dark red solid which was further purified by alumina column chromatography (CHCl<sub>3</sub>/MeOH 95.5:0.5 v/v) to afford the pure (porphyrin)Sn(OH)<sub>2</sub>.

**[5,15-Bis(4-pyridyl)-10,20-bis[2,6-bis(methoxy)phenyl]porphyrinato]tin(IV) dihydroxide (1).** A dark purple solid (151 mg, 89% yield). <sup>1</sup>H NMR (CDCl<sub>3</sub>):  $\delta$  9.13 (d, <sup>3</sup>J<sub>H-H</sub> = 4.4 Hz, 4H), 9.08 (d, <sup>3</sup>J<sub>H-H</sub> = 5.1 Hz, 4H), 9.06 (d, <sup>3</sup>J<sub>H-H</sub> = 4.4 Hz, 4H), 8.32 (d, <sup>3</sup>J<sub>H-H</sub> = 5.1 Hz, 4H), 7.84 (t, <sup>3</sup>J<sub>H-H</sub> = 8.8 Hz, 2H), 7.09 (d, <sup>3</sup>J<sub>H-H</sub> = 8.8 Hz, 4H), 3.58 (s, 12H). <sup>13</sup>C{<sup>1</sup>H} NMR (CDCl<sub>3</sub>):  $\delta$  160.43, 149.59, 148.63, 147.57, 145.63, 132.70, 132.43, 131.60, 129.92, 117.88, 117.37, 114.39, 104.41, 56.19. MS (MALDI-TOF): *m/z* = 872.0 for [M-OH]<sup>+</sup>; Calcd 870.52.

**[5,15-Bis(4-pyridyl)-10,20-bis[2,6-bis(*n*-butoxy)phenyl]porphyrinato]tin(IV) dihydroxide (2).** A dark purple solid (165 mg, 87% yield). <sup>1</sup>H NMR (CDCl<sub>3</sub>):  $\delta$  9.15 (d, <sup>3</sup>J<sub>H-H</sub> = 4.2 Hz, 4H), 9.10 (d, <sup>3</sup>J<sub>H-H</sub> = 5.9 Hz, 4H), 8.99 (d, <sup>3</sup>J<sub>H-H</sub> = 4.2 Hz, 4H), 8.34 (d, <sup>3</sup>J<sub>H-H</sub> = 5.9 Hz, 4H), 7.75 (t, <sup>3</sup>J<sub>H-H</sub> = 8.2 Hz, 2H), 7.02 (d, <sup>3</sup>J<sub>H-H</sub> = 8.2 Hz, 4H), 3.83 (t, <sup>3</sup>J<sub>H-H</sub> = 6.7 Hz, 8H), 0.87 (m, 8H), 0.40 (m, 8H), 0.17 (t, <sup>3</sup>J<sub>H-H</sub> = 8.2 Hz, 12H). <sup>13</sup>C{<sup>1</sup>H} NMR (CDCl<sub>3</sub>):  $\delta$  160.08, 149.99, 148.63, 147.96, 147.69, 145.70, 145.50, 132.73, 131.81, 119.9, 117.08, 115.24, 105.24, 68.32, 30.42, 18.30, 13.23. MS (MALDI-TOF): *m/z* = 1039.2 for [M-OH]<sup>+</sup>; Calcd 1038.8.

**[5,15-Bis(4-pyridyl)-10,20-bis[2,6-bis(*n*-octoxy)phenyl]porphyrinato]tin(IV) dihydroxide (3).** A dark purple solid (164 mg, 75% yield). <sup>1</sup>H NMR (CDCl<sub>3</sub>):  $\delta$  9.20 (d, <sup>3</sup>J<sub>H-H</sub> = 5.1 Hz, 4H), 9.17 (d, <sup>3</sup>J<sub>H-H</sub> = 4.4 Hz, 4H), 9.06 (d, <sup>3</sup>J<sub>H-H</sub> = 5.1 Hz, 4H), 8.34 (d, <sup>3</sup>J<sub>H-H</sub> = 5.1 Hz, 4H), 7.76 (t, <sup>3</sup>J<sub>H-H</sub> = 8.1 Hz, 2H), 7.02 (d, <sup>3</sup>J<sub>H-H</sub> = 8.7 Hz, 4H), 3.82 (t, <sup>3</sup>J<sub>H-H</sub> = 5.9 Hz, 8H), 0.94 (m, 8H), 0.88 (m, 8H), 0.77 (m, 8H), 0.73 (t, <sup>3</sup>J<sub>H-H</sub> = 7.4 Hz, 12H), 0.66 (m, 8H), 0.61 (m, 8H), 0.51 (m, 8H). <sup>13</sup>C{<sup>1</sup>H} NMR (CDCl<sub>3</sub>):  $\delta$  160.12, 149.65, 148.62, 147.52, 145.54, 132.80, 132.68, 131.65, 129.89, 118.56, 117.22, 115.09, 105.08, 68.71, 31.79, 29.08, 28.84, 28.55, 25.10, 22.64, 14.19. MS (MALDI-TOF): *m/z* = 1264.6 for [M-OH]<sup>+</sup>; Calcd 1263.3.

**Additional comments on the temperature-dependence of the nanoparticles synthesis.** When the reaction temperature was elevated (90 °C) under stirring conditions, porphyrin **1** resulted in crystalline particles with the similar morphology as they appeared at low temperature (45 °C) but with larger sizes (3~20 μm). In contrast, porphyrin **2** and **3** gave only amorphous materials under these same elevated-temperature conditions. These observations imply that the aggregation is a complex function of the solubility of building blocks, growth temperature, and cooling rate, among many other variables. As such, we don't necessarily expect the formation of better defined aggregates at elevated temperatures.

#### IV. UV-vis and Fluorescence Spectroscopic Data

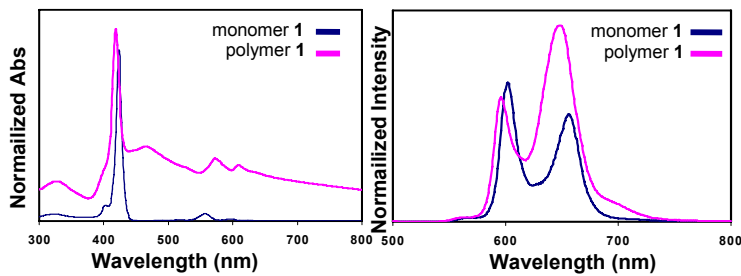


**Figure S1.** UV-vis and fluorescence spectra of **1** ( $2.5 \times 10^{-6}$  M) and nanoparticles made from **1**.

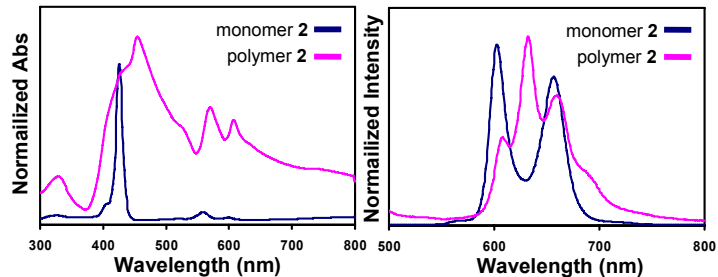


**Figure S2.** UV-vis and fluorescence spectra of **2** ( $2.0 \times 10^{-6}$  M) and nanoparticles made from **2**.

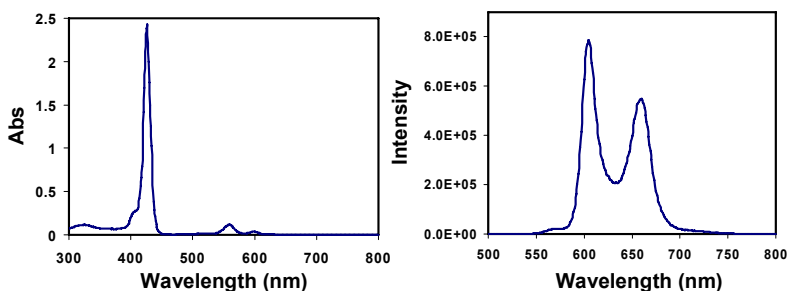


**Figure S3.** UV-vis and fluorescence spectra of **3** ( $2.3 \times 10^{-6}$  M).

## V. PXRD Data

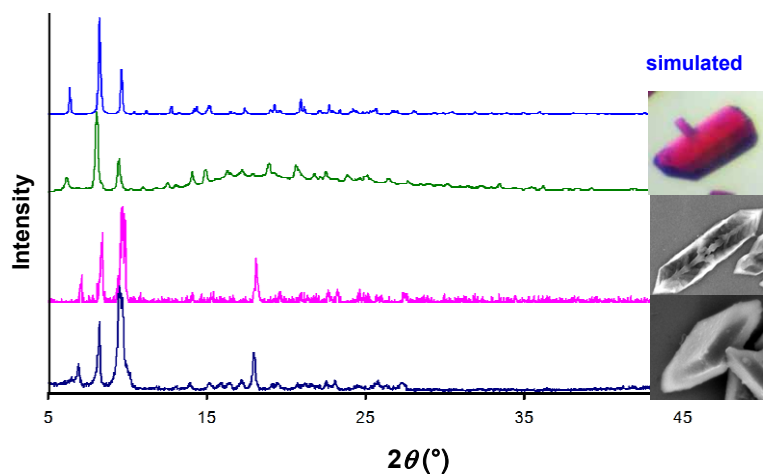


**Figure S4.** The PXRD patterns for the two nanoparticles of **2** as well as that from a single-crystal sample of **2**. Also shown is the simulated PXRD pattern obtained from the X-ray crystal structure of **2**.

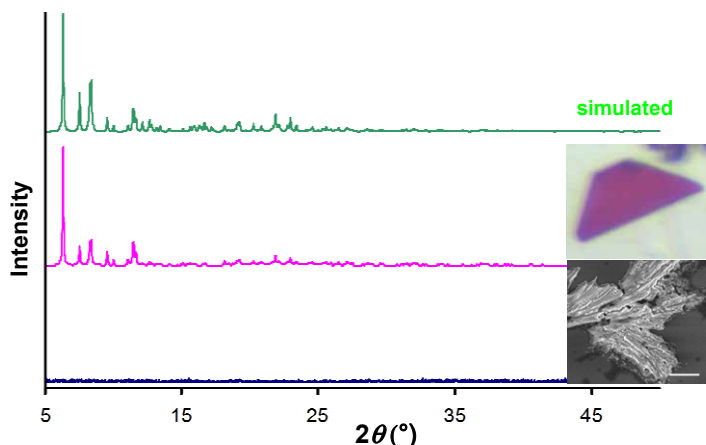


**Figure S5.** The PXRD patterns for an amorphous sample and a single-crystal sample of **3**. Also shown the simulated PXRD pattern obtained from the X-ray crystal structure of **3**.

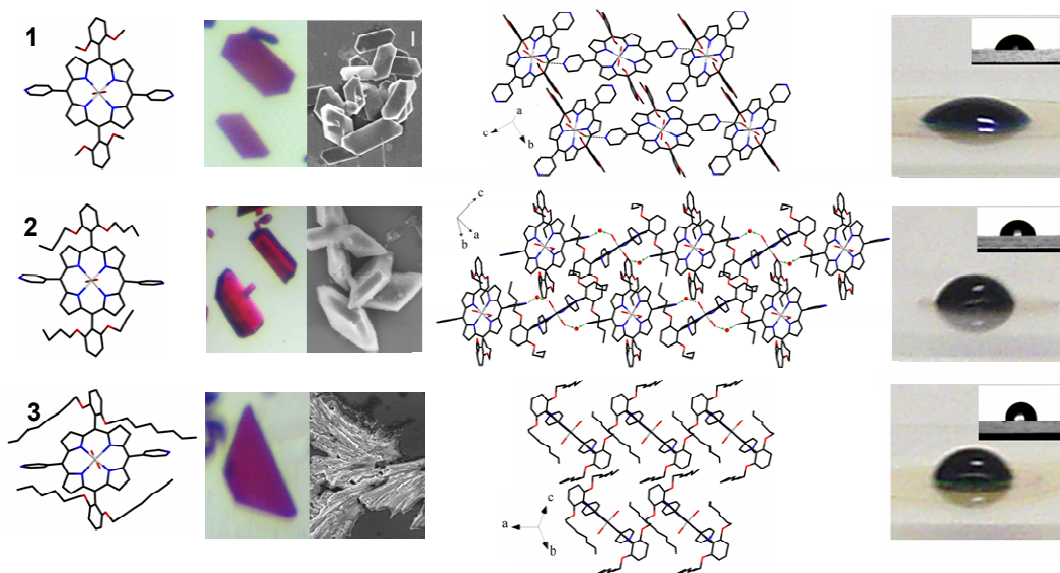


**Figure S6.** (This is the color version of Figure 3 in the manuscript.) Structural, physical, and morphological data for metalloporphyrins **1**, **2** and **3**. From the left: First column: Stick representations of the X-ray structures of the (porphyrin)Sn building blocks. Second column: Color photographs of single crystals of each of the (porphyrin)Sn compounds, and corresponding SEM images of the nanocrystals prepared under agitation. Third column: Packing diagram representations of the X-ray structures, illustrating the intramolecular H-bonding pattern between adjacent porphyrin layers in **1**, water-mediated H-bonding pattern between adjacent porphyrin layers in **2**, and the absence of such pattern for **3** (C= black, O = red, N = blue, hydrogen-bonded HO-Sn = green, hydrogen-bonded H<sub>2</sub>O = green, other hydrogen atoms are omitted for clarity). These differences lead to completely different nanoscale morphologies for **1**, **2**, and **3** under agitated growth conditions. Those that can form H-bonds (**1** and **2**) are more likely to afford well-defined nanocrystals while the porphyrin that does not (**3**) tends to yield amorphous nanoparticles. Fourth Column: The relative increase in hydrophobicity of the corresponding porphyrin thin films, as shown via contact-angle measurements (69° for **1**, 74° for **2**, and 83° for **3**) when drops of blue-colored water are placed on top of glass-supported (porphyrin)Sn(OH)<sub>2</sub> films. Insets show the side views of the water drops: the most hydrophobic film of **3** cause water to bead up the most.

## VI. Single-crystal X-ray diffraction experiments for (porphyrin)Sn(OH)<sub>2</sub>

Single crystals of **1**, **2**, and **3** were grown in air by careful layering a 1-mM ethanol solution of the respective (porphyrin)Sn(OH)<sub>2</sub> complex over water inside a glass tube (5-8 mm in diameter). The tube was then capped and allowed to reach equilibrium under darkness. Single crystals appear at the interface of the two solvents over a period of 7-14 days and were mounted for data collection immediately from solution using epoxy super glue.

A STOE IPDS 2T diffractometer was used to collect intensity data at 100 K with graphite monochromatized Mo K $\alpha$  radiation. An analytical absorption correction was performed and all structures were refined with SHELXTL software. In more details:

Structure **1** exhibited some disorder in the cavities with methanol molecules but no twin domains where found. The region between the porphyrins (cavities) was partially occupied 65(2)% with methanol molecules. The largest positive hole of 0.83 e. $\text{\AA}^{-3}$  was 0.67  $\text{\AA}$  from C47 (solvent molecule) and the largest negative hole of -0.60 e. $\text{\AA}^{-3}$  is 1.03  $\text{\AA}$  away from Sn2. Aromatic H atoms were placed in geometric positions (C-H = 0.95  $\text{\AA}$ ) using a riding model, while the coordinates of the water H atoms were refined

using geometric restraints on the O-H bond lengths and H-O-H bond angles. Crystallographic data for the refinement of structure **1** are shown in table S-1.

**Table S-1.** Crystal data and structure refinement for **1**.

Empirical formula	C <sub>49.30</sub> H <sub>50.94</sub> N <sub>6</sub> O <sub>9.65</sub> Sn
Formula weight	1000.60
Temperature	100(2) K
Wavelength	0.71073 Å
Crystal system	Triclinic
Space group	P-1
Unit cell dimensions	a = 10.6851(6) Å, α = 91.025(5)° b = 11.0810(7) Å, β = 96.897(5)° c = 19.8632(14) Å, γ = 99.681(5)°
Volume	2299.8(3) Å <sup>3</sup>
Z	2
Density (calculated)	1.445 g/cm <sup>3</sup>
Absorption coefficient	0.621 mm <sup>-1</sup>
F(000)	1032
Crystal size	0.55 x 0.45 x 0.40 mm <sup>3</sup>
Theta range for data collection	4.09 to 28.00°
Index ranges	-14<=h<=14, -14<=k<=14, -26<=l<=26
Reflections collected	16677
Independent reflections	11031 [R <sub>int</sub> = 0.0960]
Completeness to θ = 28.00°	95%
Refinement method	Full-matrix least-squares on F <sup>2</sup>
Data / restraints / parameters	7218 / 1 / 571
Goodness-of-fit on F <sup>2</sup>	1.081
Final R indices [>2sigma(I)]	R <sub>obs</sub> = 0.0765, wR <sub>obs</sub> = 0.1471
R indices (all data)	R <sub>all</sub> = 0.1352, wR <sub>all</sub> = 0.1667
Extinction coefficient	0.0073(9)
Largest diff. peak and hole	0.834 and -0.604 e.Å <sup>-3</sup>

R =  $\sum ||F_o|| - |F_c|| / \sum |F_o|$ , wR =  $\{\sum [w(|F_o|^2 - |F_c|^2)^2] / \sum [w(|F_o|^4)]\}^{1/2}$  and calc w=1/[σ<sup>2</sup>(F<sub>o</sub><sup>2</sup>)+(0.0674P)<sup>2</sup>+3.9716P] where P=(F<sub>o</sub><sup>2</sup>+2F<sub>c</sub><sup>2</sup>)/3

The buoxy-groups of structure **2** were found to be heavily disordered. Furthermore, the porphyrin packing created merohedral twin domains in the ac-plane. All four mounted crystals of **2** were tested and showed the same type of disorder and twinning although no visual evidence were found from the reciprocal space such as split or diffuse intensity reflections. Although the R-value was around 10% when being refined with a twin law, the structure did not make sense chemically because electron density was delocalized (diffuse) around Sn atoms, which apparently were located at the right crystallographic position.

A twin law of 180 degrees rotation along b-axis [-1 0 0 0 1 0 0 0 -1] gave a refined twin fraction of 12.2(2)% for a chemically reasonable structure. The absolute structure parameter (flack) for the first twin domain was 32(2)% and for the second twin domain 38.3(3)%. Aromatic H atoms were placed in geometric positions (C-H = 0.95 Å) using a riding model. All water molecules in the structure were heavily disordered and delocalized. No water H atoms were found by Fourier difference maps. The distance between oxygen (on the Sn) and nitrogen (from the phenyl ring) was found around 4.14 Å comparable to the reported distance.<sup>2</sup> The largest positive hole of 1.51 e.Å<sup>-3</sup> was 0.13 Å from Sn1 and the largest negative hole of -1.38 e.Å<sup>-3</sup> is 0.75 Å away from Sn4. Crystallographic data for the refinement of structure **2** are shown in table S-2.

**Table S-2.** Crystal data and structure refinement for **2**.

Empirical formula	C <sub>239.15</sub> H <sub>136</sub> N <sub>24</sub> O <sub>29.46</sub> Sn <sub>4</sub>
Formula weight	4291.64
Temperature	100(2) K
Wavelength	0.71073 Å
Crystal system	Triclinic
Space group	P1
Unit cell dimensions	a = 18.6366(5) Å, α = 89.961(2)° b = 21.2003(6) Å, β = 101.735(2)° c = 14.3509(4) Å, γ = 90.011(2)°
Volume	5551.5(3) Å <sup>3</sup>
Z	1
Density (calculated)	1.284 g/cm <sup>3</sup>
Absorption coefficient	0.517 mm <sup>-1</sup>
F(000)	2175
Crystal size	0.52 x 0.40 x 0.38 mm <sup>3</sup>
Theta range for data collection	4.08 to 29.26°
Index ranges	-25<=h<=25, -29<=k<=29, -19<=l<=19
Reflections collected	80752
Independent reflections	49017 [R <sub>int</sub> = 0.0520]
Completeness to θ = 29.26°	97%
Refinement method	Full-matrix least-squares on F <sup>2</sup>
Data / restraints / parameters	49017 / 64 / 1033
Goodness-of-fit on F <sup>2</sup>	1.042
Final R indices [ $>2\sigma(I)$ ]	R <sub>obs</sub> = 0.0788, wR <sub>obs</sub> = 0.1914
R indices (all data)	R <sub>all</sub> = 0.1242, wR <sub>all</sub> = 0.2308
Largest diff. peak and hole	1.507 and -1.381 e.Å <sup>-3</sup>

R =  $\sum ||F_o - |F_c|| / \sum |F_o|$ , wR =  $\{\sum [w(|F_o|^2 - |F_c|^2)^2] / \sum [w(|F_o|^4)]\}^{1/2}$  and calc w=1/[σ<sup>2</sup>(Fo<sup>2</sup>)+(0.1038P)<sup>2</sup>+22.4949P] where P=(Fo<sup>2</sup>+2Fc<sup>2</sup>)/3

Structure **3** had the same type of disorder as structure **2**. The octoxy groups were disordered and a merohedral 8.4(2)% twin fraction was found after the application of a twin law of 180 degrees rotation along c-axis [-1 0 0 0 -1 0 0.791 1.083 1]. Aromatic H atoms were placed in geometric positions (C-H = 0.95 Å) using a riding model. Crystallographic data of the refinement of structure **3** are shown in table S-3.

**Table S-3.** Crystal data and structure refinement for **3**.

Empirical formula	C <sub>164</sub> H <sub>218</sub> N <sub>12</sub> O <sub>16</sub> Sn <sub>2</sub>
Formula weight	2850.88
Temperature	100.0(3) K
Wavelength	0.71073 Å
Crystal system	Triclinic
Space group	P-1
Unit cell dimensions	a = 11.2740(4) Å, α = 106.738(2)° b = 14.8228(5) Å, β = 96.679(3)° c = 24.8765(8) Å, γ = 101.290(3)°
Volume	3837.4(2) Å <sup>3</sup>
Z	1
Density (calculated)	1.234 g/cm <sup>3</sup>
Absorption coefficient	0.391 mm <sup>-1</sup>
F(000)	1514
Crystal size	0.30 x 0.24 x 0.17 mm <sup>3</sup>
Theta range for data collection	1.87 to 26.76°
Index ranges	-14<=h<=14, -18<=k<=18, -31<=l<=31
Reflections collected	58260
Independent reflections	16256 [R <sub>int</sub> = 0.0946]
Completeness to θ = 26.76°	100%
Refinement method	Full-matrix least-squares on F <sup>2</sup>
Data / restraints / parameters	16256 / 0 / 468
Goodness-of-fit on F <sup>2</sup>	1.046
Final R indices [>2sigma(I)]	R <sub>obs</sub> = 0.0638, wR <sub>obs</sub> = 0.2868
R indices (all data)	R <sub>all</sub> = 0.0822, wR <sub>all</sub> = 0.2984
Extinction coefficient	0.0055(6)
Largest diff. peak and hole	0.804 and -0.396 e.Å <sup>-3</sup>

R =  $\Sigma ||F_o| - |F_c|| / \Sigma |F_o|$ , wR =  $\{\Sigma [w(|F_o|^2 - |F_c|^2)^2] / \Sigma [w(|F_o|^4)]\}^{1/2}$  and calc w=1/[σ<sup>2</sup>(Fo<sup>2</sup>)+(0.0524P)<sup>2</sup>+147.8472P]  
 where P=(Fo<sup>2</sup>+2Fc<sup>2</sup>)/3

## VII. References

- 10
1. S. J. Lee, K. L. Mulfort, X. Zuo, A. J. Goshe, P. J. Wesson, S. T. Nguyen, J. T. Hupp and D. M. Tiede, *J. Am. Chem. Soc.* 2008, **130**, 836-838.
  2. H. J. Jo, S. H. Jung, H.-J. Kim, *Bull. Korean Chem. Soc.* 2004, **25**, 1869-1873.